Physica C 470 (2010) 313–317

Contents lists available at ScienceDirect

Physica C

journal homepage: www.elsevier.com/locate/physc

Superconductivity of Ni-doping 2*H*–TaS_2

L.J. Li [a], X.D. Zhu [a,b], Y.P. Sun [a,b,*], H.C. Lei [a], B.S. Wang [a], S.B. Zhang [a], X.B. Zhu [a], Z.R. Yang [a], W.H. Song [a]

[a] Key Laboratory of Materials Physics, Institute of Solid State Physics, Chinese Academy of Sciences, Hefei 230031, People's Republic of China
[b] High Magnetic Field Laboratory, Chinese Academy of Sciences, Hefei 230031, People's Republic of China

ARTICLE INFO

Article history:
Received 20 November 2009
Accepted 16 January 2010
Available online 25 January 2010

Keywords:
Superconductivity
Single crystals
Charge density wave

ABSTRACT

The superconductivity of 2*H*–Ni_xTaS_2 single crystals with Ni-doping content of $0 \leqslant x \leqslant 0.08$ is investigated. Compared with the temperature dependence of resistivity $\rho(T)$ curve of un-doped 2*H*–TaS_2 with charge density wave (CDW) transition ($T_{CDW} = 78$ K), no sign of CDW is observed for Ni-doping sample Ni_xTaS_2, meaning the suppression of CDW caused by Ni-doping. The increase of superconducting critical temperature T_C caused by Ni-doping is observed and the optimal Ni-doping content corresponding to the maximum zero resistance temperature $T_{Czero}^{max} = 4.15$ K is $x = 0.04$. The superconductivity of $Ni_{0.04}TaS_2$ is investigated in detail. The obtained superconducting parameters indicated that $Ni_{0.04}TaS_2$ is an intermediate coupling anisotropic type-II superconductor with anisotropy ratio $\gamma = H_{c2}^{ab}(T)/H_{c2}^{c}(T) \approx 3.58$.

1. Introduction

Layered transition-metal dichalcogenides (TMDC's) of the type MX_2 (M is the transition metal, X = S, Se, Te) have been extensively studied for their rich electronic properties due to low dimensionality [1]. Each layer of TMDC's consists of a hexagonal transition metal sheet sandwiched by two similar chalcogen sheets, which can be regarded as stacking of covalent coupling X–M–X sandwiches, and the coupling between sandwiches being of weak van der Waals type. Charge density wave (CDW) and superconductivity coexist in most these materials such as 2*H*–$TaSe_2$, 2*H*–$NbSe_2$, 2*H*–TaS_2, 4*Hb*–TaS_2, and 4*Hb*–$TaSe_2$ [2–4]. The electron–phonon coupling and its relationship with the CDW have been investigated by angle resolved photoemission in 2*H*–$TaSe_2$ and 2*H*–$NbSe_2$ systems [5–7]. It is found that the CDW transition temperature decreases and meanwhile the superconducting critical temperature (T_C) increases, in $TaSe_2$ and TaS_2, which indicates that these two kinds of quantum orders (CDW and superconductivity) compete with each other [8–10]. CDW and superconductivity are two very different cooperative electronic phenomena, and yet both occur because of Fermi surface instabilities and electron–phonon coupling. CDW represents the periodic modulation of the charge density in solids, which is usually found in low-dimensional materials. 2*H*–TaS_2, a classic, layered TMDC, undergoes a CDW transition at ~78 K and a superconducting transition at ~0.8 K [1,2].

The intercalation effects in TaS_2 have attracted extensive efforts during the past decades [11–14]. With 3d-transitional metal (3d-TM) intercalation, enhancement of superconductivity and suppression of CDW has been observed in $Fe_{0.05}TaS_2$ [15], and copper intercalated Cu_xTaS_2 polycrystalline samples [16] and single crystals [17]. Very recently, the raise of T_C within low Ni-doping content $Ni_{0.05}TaS_2$ single crystals have been also observed [18]. In this paper, Ni_xTaS_2 single crystals with different Ni-doping content of $0 \leqslant x \leqslant 0.08$ are grown and their superconductivities are systemically investigated by the magnetic, electronic and heat transport experiments. For $Ni_{0.04}TaS_2$ single crystal with the maximum T_C its superconducting parameters are obtained.

2. Experimental

2*H*–Ni_xTaS_2 single crystals with $x = 0$, 0.02, 0.04, 0.05, 0.06, and 0.08 were grown using the NaCl/KCl flux method [19]. The room temperature crystal structure and lattice constants were determined by powder and single crystal X-ray diffraction (XRD) (Philips X'pert PRO) using Cu Kα radiation. To perform the powder XRD experiment, several single crystals were crushed to powder. Magnetization measurements were performed in a Quantum Design (QD) superconducting quantum interference device (SQUID) MPMS system ($1.8 \leqslant T \leqslant 400$ K, $0 \leqslant H \leqslant 5$ T). Resistivity measurements were carried out by the standard four-probe method in the temperature range of 1.8–300 K in a commercial QD Physical Property Measurement System (PPMS, $1.8 \leqslant T \leqslant 400$ K, $0 \leqslant H \leqslant 9$ T). Specific heat was measured by the thermal relaxation method (QD, PPMS) in the temperature range of 2–15 K.

* Corresponding author. Address: Key Laboratory of Materials Physics, Institute of Solid State Physics, Chinese Academy of Sciences, Hefei 230031, People's Republic of China. Tel.: +86 551 559 2757; fax: +86 551 559 1434.
E-mail address: ypsun@issp.ac.cn (Y.P. Sun).

0921-4534/$ - see front matter © 2010 Elsevier B.V. All rights reserved.
doi:10.1016/j.physc.2010.01.042

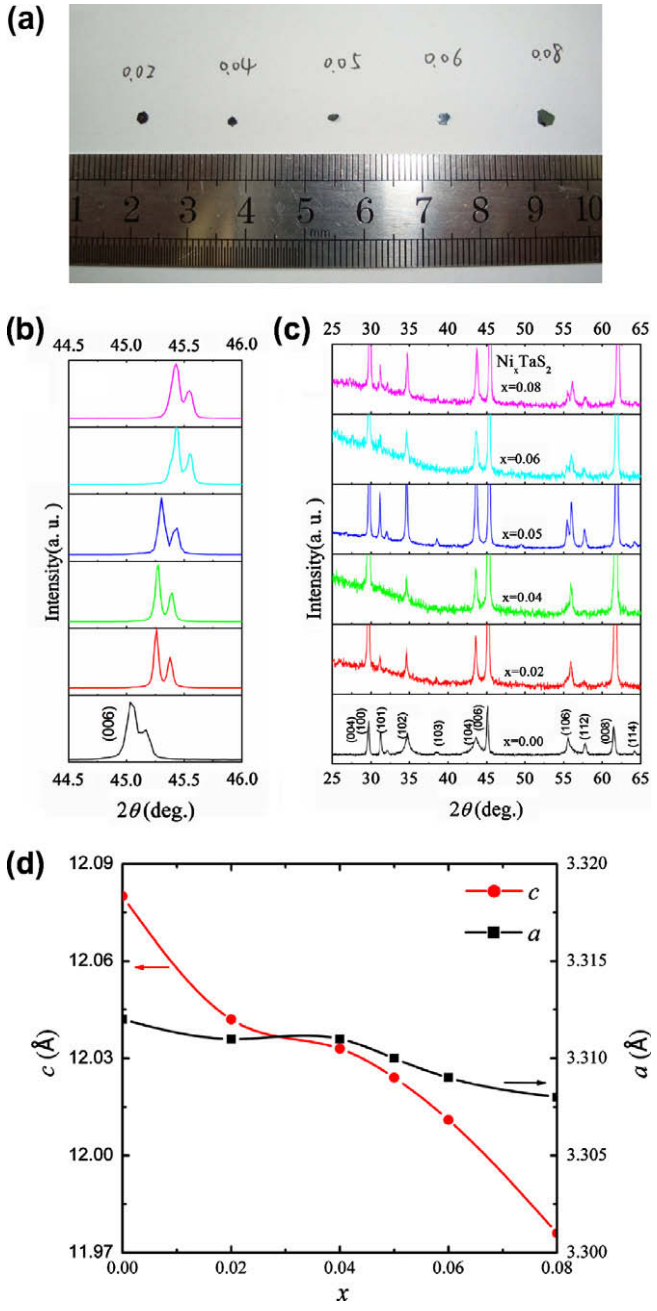

Fig. 1. (a) The photograph of Ni_xTaS_2 single crystals. (b) The magnification plot of (0 0 6) peak of Ni_xTaS_2 single crystals. (c) The powder XRD patterns of crushed single crystals. (d) The curve of the lattice constants a and c as a function of Ni-doping level in Ni_xTaS_2 single crystals.

3. Results and discussion

Fig. 1a[1] shows the typical single crystal photos. The grown crystals are dark blue, mirror-like plates with a typical size of $1.5 \times 1.5 \times 0.2$ mm^3. The structures of the single crystals are determined by XRD pattern. The XRD patterns for Ni_xTaS_2 single crystals with $x = 0$, 0.02, 0.04, 0.05, 0.06, and 0.08 indicates that the orientations of the crystal surfaces are perpendicular to (0 0 1) plane. The magnified plot of (0 0 6) peak is displayed in Fig. 1b. Obviously, the (0 0 6) peak position shifts to high angle with increasing Ni-doping content, implying the decrease of the c-axis lattice constant. In order to obtain the lattice constants of Ni-doped samples, the powder XRD patterns of crushed single crystals are shown in Fig. 1c, and all the peaks can be well indexed to the 2H structure, meaning Ni-doping does not change the crystal structure of 2H–TaS_2. The lattice constants obtained by fitting powder XRD patterns are shown in Fig. 1d. It shows that the Ni-doping almost does not change the value of the lattice constant a, while it obviously reduces the lattice constant c. That is to say, the Ni-doping causes the shrinkage of the lattice along the c-axis direction, which is in contrast to the expansion of the lattice along c-axis direction caused by Cu-intercalation in Cu_xTaS_2 [16,17]. Considering the smaller ion radius of Ni compared with Ta ions, the reduction of lattice constant c suggests that Ni ions do not occupy the intercalation position S–Ta–S interlayer and but substitute on the position of Ta in S–Ta–S layer. The reason why Cu and Ni ions occupy different positions in 2H–TaS_2 lattice needs to be examined further.

In order to investigate the effect of Ni-doping on the CDW transition, the temperature dependence of the in-plane resistivity $\rho_{ab}(T)$ of Ni_xTaS_2 single crystals is measured. In Fig. 2a we plots the resistivity $\rho_{ab}(T)$ for Ni_xTaS_2 as a function of temperature under zero field in the temperature range of 2–280 K. It shows that $\rho_{ab}(T)$ almost follows a linear temperature dependence with no obvious change of curvature (like a kink) corresponding to the CDW transition observed in the high temperature region. That is to say, the CDW transition occurring at $T_{CDW} = 78$ K for 2H–TaS_2 is suppressed by Ni-doping, even if Ni-doping content is only 2%. Compared with

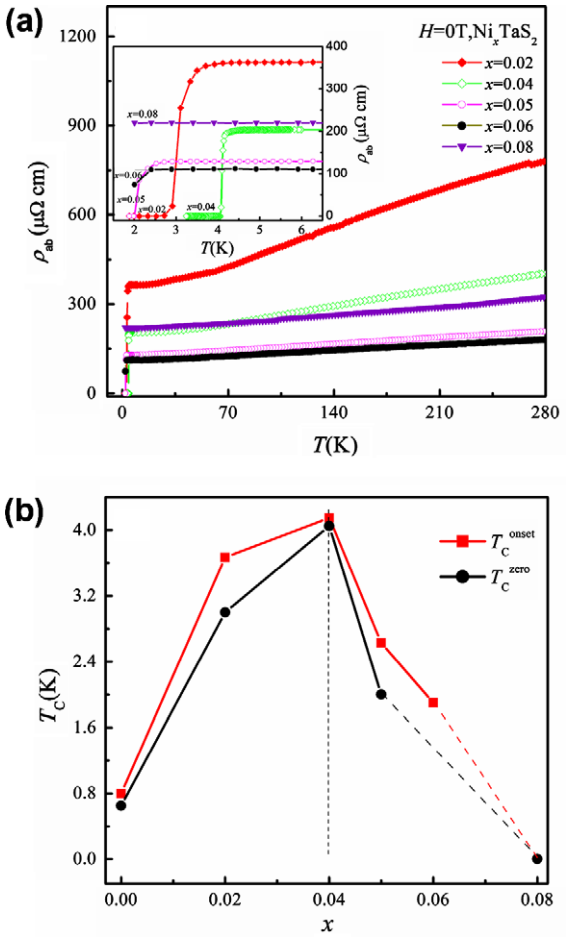

Fig. 2. (a) The temperature dependence of the resistivity $\rho_{ab}(T)$ for Ni_xaS_2. The inset shows the enlarged view of the low temperature part. (b) The Ni-doping level dependence of T_c^{onset} and T_c^{zero}.

[1] For interpretation of color in Figs. 1–7, the reader is referred to the web version of this article.

the result of Cu-intercalated Cu_xTaS_2 single crystals [17], the CDW suppression of 2*H*–TaS_2 caused by the partial substitution of Ni for Ta is more efficient than that caused by the Cu-intercalation between S–Ta–S layers. In the low temperature region, Fig. 2a shows that Ni_xTaS_2 single crystals display a superconducting transition except for the sample of $x = 0.08$, that can be clearly seen in the enlarged plot in low temperature region given in the inset of Fig. 2a although zero resistance is not reached for $x = 0.06$ sample down to 2 K. The onset superconducting transition temperature T_C^{onset} and zero resistance temperature T_C^{zero} as a function of Ni-doping content x is shown in Fig. 2b. Compared with the parent 2*H*–TaS_2 with $T_C = 0.8$ K, Fig. 2b indicates that a small amount of Ni-doping ($x \leqslant 0.06$) clearly enhances the superconducting transition temperature and the optimal Ni-doping content takes place at $x = 0.04$. This raise of superconducting transition temperature may be related to the change of the density of states near the Fermi surface caused by Ni-doping.

To confirm the presence of bulk superconductivity in Ni-doping single crystals, the magnetization is measured using the dc susceptibility method. In Fig. 3, we present the temperature-dependent dc susceptibility data of $x = 0.02$ and 0.04 samples measured with a dc field of 10 Oe using the zero-field-cooling (ZFC) and field-cooling (FC) modes, in which the direction of dc field is perpendicular to the *ab*-plane of the single crystals. The T_C^{onset} determined from the dc magnetization is about 3.17 K and 4.19 K for $x = 0.02$ and 0.04 samples, respectively, which is consistent with the zero resistance temperature as determined from $\rho_{ab}(T)$ curves. Therefore, combining the results of resistivity and dc magnetization, it can be concluded that a small amount of Ni-doping indeed gives rise to the enhancement of bulk superconductivity of Ni_xTaS_2 samples.

In order to obtain the superconducting parameters of Ni_xTaS_2, the $x = 0.04$ single crystal with the optimal Ni-doping is selected to perform a detailed measurement. Firstly, the lower critical fields H_{c1} is determined by measuring the initial magnetization curve of the sample $Ni_{0.04}TaS_2$ at fixed temperature under the ZFC mode with the field direction along the *ab*-plane ($H||ab$) (Fig. 4a) and *c*-axis ($H||c$) (Fig. 4b). Due to the plate shape of the single crystal sample, the demagnetization effect for $H||ab$ is negligible, while the demagnetization for $H||c$ is large [19]. The corrected data are plotted in Fig. 4b. Obviously, Fig. 4a and b shows that the initial $M(H)$ is linear. H_{c1} is determined as the point deviating from linearity based on the criterion $\Delta M = (M_m - M_{th}) < 10^{-5}$ emu, here, M_m is the measuring moment value and M_{th} is inner differential moment value. From Fig. 4a and b, both H_{c1}^{ab} and H_{c1}^{c} values at the

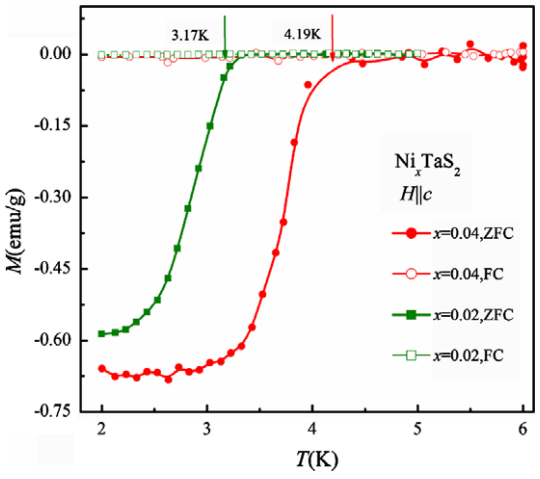

Fig. 3. The temperature dependence of the dc magnetization of $x = 0.02$ and 0.04 samples under the ZFC and FC measuring modes with $H = 10$ Oe.

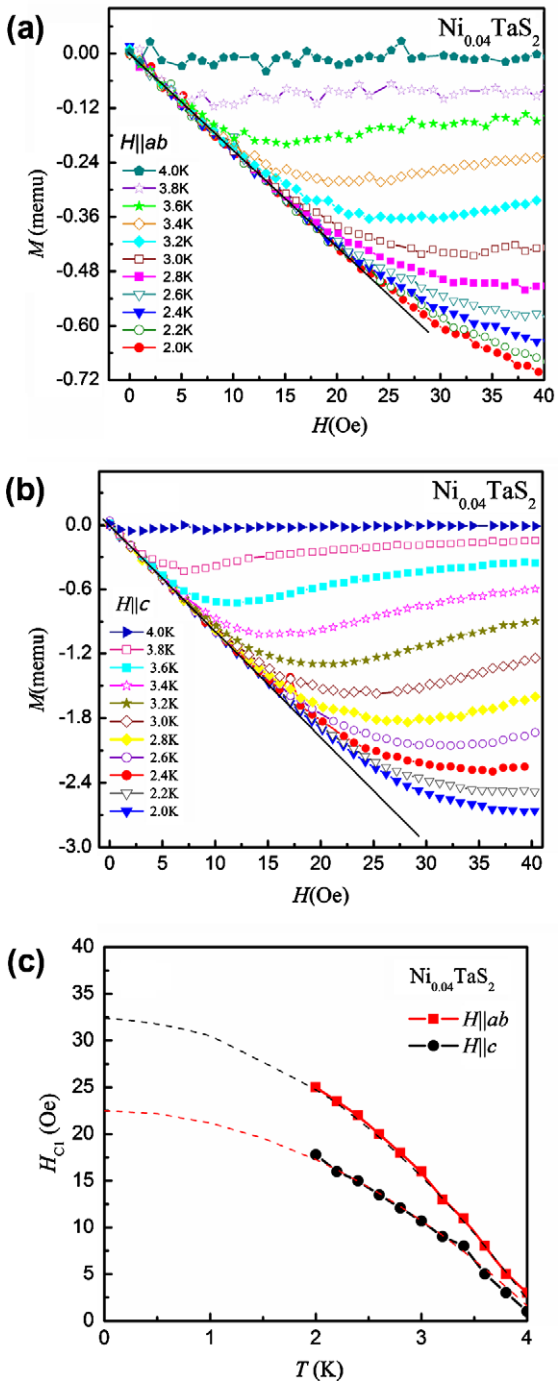

Fig. 4. (a) The ZFC $M(H)$ isotherms for field $H||ab$ of $Ni_{0.04}TaS_2$ at the different temperatures. (b) The ZFC $M(H)$ isotherms for field $H||c$ of $Ni_{0.04}TaS_2$ at the different temperatures. (c) The temperature dependence of the lower critical field (H_{c1}) for $Ni_{0.04}TaS_2$. The dashed lines are the fitted curves.

different temperatures can be obtained as shown in Fig. 4c. It shows that the temperature dependence of $H_{c1}^{ab}(T)$ and $H_{c1}^{c}(T)$ can be fitted according to $H_{c1}(T) = H_{c1}(0)[1 - (T/T_C)^2]$ as shown by the dashed lines in Fig. 4c [20]. Based on the fitting, the obtained zero temperature $H_{c1}^{ab}(0)$ and $H_{c1}^{c}(0)$ are 32.4 Oe and 22.5 Oe.

Secondly, the upper critical field H_{c2} is determined by measuring the resistance transition at different fields with the field direction along the *ab*-plane (Fig. 5a) and *c*-axis (Fig. 5b). It shows that $\rho_{ab}(T)$ curve shifts in almost parallel fashion down to lower temperatures with increasing applied magnetic fields. The H_{c2} for both

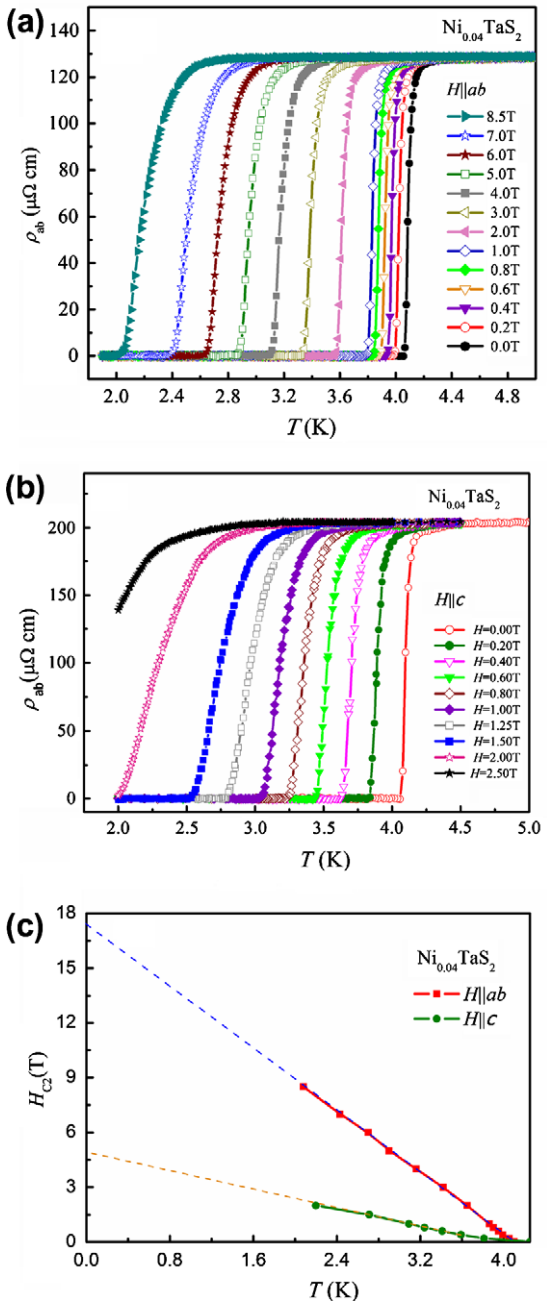

Fig. 5. The temperature-dependent resistivity of $Ni_{0.04}TaS_2$ single crystal at different magnetic fields applied parallel *ab* (a) and perpendicular to *ab* (b). (c) The temperature dependence of the upper critical field (H_{c2}) for $Ni_{0.04}TaS_2$. The dashed line represents the linear fitting near T_C according to WWH formula.

$H||ab$ and $H||c$ directions are determined by the midpoint of $\rho_{ab}(T)$ curves. The temperature dependence of the upper critical field $H_{c2}(T)$ curve is shown in Fig. 5c, exhibiting as almost a linear temperature dependence near T_C. The zero temperature value of $H_{c2}(0)$ can be determined according to the Werthamer–Helfand–Hohenberg (WHH) formula [21]: $H_{c2}(0) = -0.693T_C\left(\frac{dH_{c2}}{dT}\right)_{T=T_C}$, when dH_{c2}/dT is the slope of $H_{c2}(T)$ near T_C. Using the WHH formula the zero temperature values of the upper critical fields are calculated to be $H_{c2}^{\|ab}(0) = 17.3$ T and $H_{c2}^{\|c}(0) = 4.85$ T. In the framework of the Ginzburg–Landau (GL) theory, it is known that $H_{c2}^{ab}(0) = \Phi_0/2\pi\xi_{ab}(0)\xi_c(0)$ and $H_{c2}^{c}(0) = \Phi_0/2\pi\xi_{ab}^2(0)$, where Φ_0 is the flux quantum. From the relations the zero temperature values of the GL coherence length can be determined to be $\xi_{ab}(0) = 8.24$ nm and $\xi_c(0) = 2.31$ nm, respectively. The GL parameters $\kappa_i(0)$ are obtained using the equation $H_{c2}^i(0)/H_{c1}^i(0) = 2\kappa_i^2(0)/\ln\kappa_i(0)$ (where i denotes the field applied along i direction). The thermodynamic critical field $H_c(0)$ can be estimated to be 0.2 T by using the equation: $H_c(0) = H_{c1}^{ab}(0)\sqrt{2}\kappa_{ab}(0)/\ln\kappa_{ab}(0)$. The GL penetration lengths are evaluated by the equations: $\kappa_c(0) = \lambda_{ab}(0)/\xi_{ab}(0)$ and $\kappa_{ab}(0) = \lambda_{ab}(0)/\xi_c(0) = [\lambda_{ab}(0)\lambda_c(0)/\xi_{ab}(0)\xi_c(0)]^{1/2}$. The anisotropy is $\gamma_{anis} = H_{c2}^{\|ab}(0)/H_{c2}^{\|c}(0) = \xi_{ab}(0)/\xi_c(0) = 3.6$, which is a little less than that of $Cu_{0.03}TaS_2$ single crystal [22].

The specific heat divided by temperature, C/T, for $Ni_{0.04}TaS_2$ as a function of T^2 at $H = 0$ T is shown in Fig. 6. It displays a jump in the C/T–T^2 curve at 4.14 K, which is indicative of the bulk superconducting transition. The critical temperature from the specific heat data defined as the midpoint of the transition (T_c^{mid}) is determined to be 3.99 K, which is close to the critical temperature obtained from the magnetic and electron transport data.

Usually, the total specific heat C is assumed to be composed of the electron and lattice parts $C(T) = C_e(T) + C_{ph}(T)$. In the normal state, the specific heat of the lattice part is expressed by the βT^3 term at temperatures much below the Debye temperature Θ_D and the electronic specific heat is assumed to be the γT term, i.e. $C/T = \gamma + \beta T^2$. From the fitting of the specific heat data in the normal state indicated by the black line of Fig. 6, γ and β values are obtained to be 13.02 mJ mol^{-1} K^{-2} and 0.39 mJ mol^{-1} K^{-4}. The value of Θ_D is calculated to be 244 K using the formula $\Theta_D = \left(\frac{n\times 1.944\times 10^6}{\beta}\right)^{1/3}$, where n is the number of elements per formula unit. Compared with the parent $2H$–TaS_2 with $\gamma = 8.5$ mJ mol^{-1} K^{-2} and $\beta = 0.37$ mJ mol^{-1} K^{-4} (shown in Table 1) [22], the value of γ for $Ni_{0.04}TaS_2$ is slightly larger, while the value of β is almost the same.

In order to estimate the electron–phonon coupling constant λ_{e-ph}, the McMillan equation is used,

$$\lambda_{e-ph} = \frac{\mu^* ln\left(\frac{1.45T_C}{\Theta D}\right) - 1.04}{1.04 + ln\left(\frac{1.45T_C}{\Theta D}\right)(1 - 0.62\mu^*)},$$

the Coulomb pseudopotential $\mu^*$is being assumed to be 0.15 empirically. The value of λ_{e-ph} is determined to be <0.68, which is less than the minimum value "1" of strong coupling, meaning that the $Ni_{0.04}TaS_2$ is to be classified into an intermediate or weak coupling BCS superconductor.

The electronic specific heat C_{es} in the superconducting state is obtained by subtracting the lattice contribution estimated from the total specific heat. The temperature dependence of C_{es}/T for

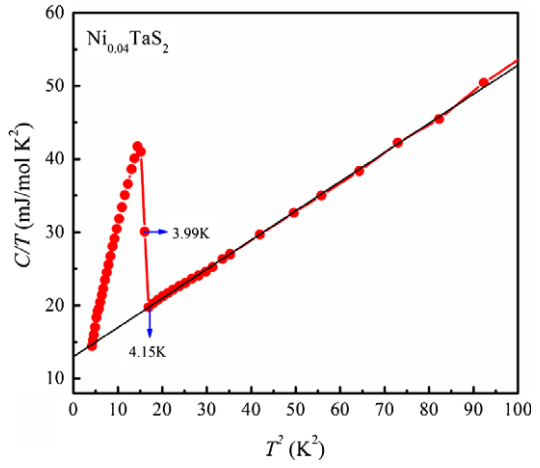

Fig. 6. Specific heat divided by temperature (C/T) as a function of T^2 for $Ni_{0.04}TaS_2$ measured at $H = 0$. The black line is the fitting results.

Table 1
Superconducting parameters of 2*H*–$Ni_{0.04}TaS_2$, 2*H*–TaS_2 and 2*H*–$Cu_{0.03}TaS_2$.

	T_C (K)	λ_n (mJ mol^{-1} K^{-2})	β (mJ mol^{-1} K^{-4})	$\Delta C/\gamma_n T_C$	Ref.
$Ni_{0.04}TaS_2$	4.15	13.02	0.398	1.762	This work
2*H*–TaS_2	0.8	8.5	0.37	1.9	[19]
$Cu_{0.03}TaS_2$	4.03	10.8	0.39(3)	1.64	[25]

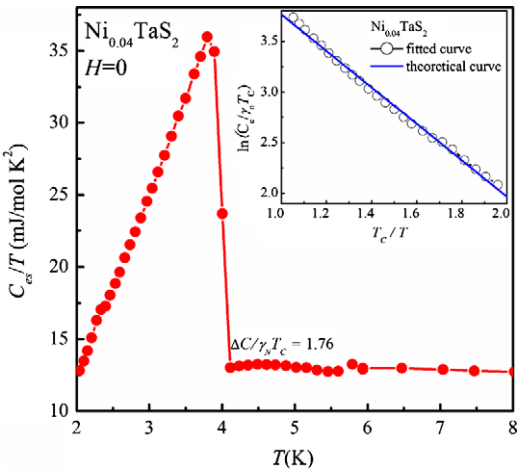

Fig. 7. Electronic specific heat divided by temperature (C_{es}/T) as a function of T for $Ni_{0.04}TaS_2$ measured at $H = 0$. The solid line in the inset shows C_{es}/T calculated by assuming an isotropic s-wave BCS gap with $2\Delta/k_BT_C = 3.6$.

Table 2
Superconducting parameters for $Ni_{0.04}TaS_2$: critical temperature for superconductivity T_C, lower critical field $H_{c1}(0)$ (after demagnetization correction), upper critical field $H_{c2}(0)$, thermodynamic critical field $H_c(0)$, GL parameters $\kappa(0)$, GL coherence length $\xi(0)$, penetrated depth λ, GL anisotropy ratio γ_{anis}, electronic specific heat coefficient γ, lattice specific heat coefficient β, debye temperature Θ_D, specific heat jump $\Delta C/\gamma_n T_C$, and gap ratio $2\Delta/k_BT_C$.

		H||*ab*	*H*||*c*
T_C (K)	4.15		
H_{c1} (Oe)		32.4	22.5
H_{c2} (T)		17.3	4.85
H_c (T)	0.2		
κ (0)		112.98	67.36
ξ (nm)		8.24	2.31
λ (nm)		555.05	1980
γ_{anis}	3.58		
γ (mJ mol^{-1} K^{-2})	13.02		
β (mJ mol^{-1} K^{-4})	0.398		
λ_{e-ph}	0.68		
Θ_D (K)	244		
$\Delta C/\gamma_n T_C$	1.762		
$2\Delta/k_BT_C$	3.6		

$Ni_{0.04}TaS_2$ is plotted in Fig. 7. Below the superconducting transition temperature, the temperature dependence of the electronic specific heat cannot be fitted by a T^n function, but it follows an exponential decay as shown in the inset of Fig. 7. From the obtained $\ln(C_{es}/\gamma T_C)$ versus T_C/T data shown in the inset of Fig. 7, the ratio of the gap at the critical temperature is sound to be about $2\Delta/k_BT_C = 3.6$ by using the relation $C_{es} \sim \exp\left(\frac{-\Delta(T)}{k_BT}\right)$, which is slightly larger than the BCS value (3.53) in the weak coupling limit [15]. The solid line in the inset of Fig. 7 is the theoretical result of the isotropic s-wave BCS gap with $2\Delta/k_BT_C = 3.6$, demonstrating that it is in good agreement with the experimental data. The extracted specific heat jump at $T_C(\Delta C/\gamma T_C = 1.76)$ is also larger than the weak coupling value 1.43, meaning an intermediate coupling [23]. This value is slightly larger than $\Delta C/\gamma T_C = 1.64$ observed for $Cu_{0.03}TaS_2$, although it is obviously less than the extant value of 1.9 for the parent sample 2*H*–TaS_2 [22].

4. Conclusion

In summary, the effect of Ni-doping content on the CDW transition and superconductivity of 2*H*–Ni_xTaS_2 single crystals is investigated. It is found that a small amount of Ni-doping level can obviously suppress the CDW transition and enhance the superconductivity of 2*H*–TaS_2, which may originate from the change of the density of states (DOS) near the Fermi surface caused by Ni-doping. The anisotropic superconducting state parameters of $Ni_{0.04}TaS_2$ have been determined (shown in Table 2). The value of electron–phonon coupling constant λ_{e-ph} is determined to be <0.68 that is less than the minimum value 1 of strong coupling, and the specific heat jump at $T_C(\Delta C/\gamma T_C = 1.76)$ is also larger than the weak coupling value 1.43. Those results definitely show that $Ni_{0.04}TaS_2$ is an anisotropic, intermediate coupling, II type BCS superconductor.

Acknowledgments

This work is supported by the National Key Basic Research under Contract No. 2006CB601005, 2007CB925002, and the National Nature Science Foundation of China under Contract No.10774146, 10774147 and Director's Fund of Hefei Institutes of Physical Science, Chinese Academy of Sciences.

References

[1] L.F. Mattheiss, Phys. Rev. B 8 (1973) 3719.
[2] J.M.E. Harper, T.H. Geballe, F.J. Di Salvo, Phys. Rev. B 15 (1977) 2943.
[3] F.J. Di Salvo, D.E. Moncton, J.V. Waszczak, Phys. Rev. B 14 (1976) 4321.
[4] M. Holt, P. Zschack, Hawoong Hong, M.Y. Chou, T.-C. Chiang, Phys. Rev. Lett. 86 (2001) 3799.
[5] J.A. Wilson, Phys. Rev. B 15 (1977) 12.
[6] R.M. Fleming, D.E. Moncton, D.B. McWhan, F.J. DiSalvo, Phys. Rev. Lett. 45 (1980) 7.
[7] T. Valla, A.V. Fedorov, P.D. Johnson, J. Xue, K.E. Smith, F.J. DiSalvo, Phys. Rev. Lett. 85 (2000) 22.
[8] J.A. Wilson, A.D. Yoffe, Adv. Phys. 28 (1969) 193.
[9] J.A. Wilson, F.J. Di Salvo, S. Mahajan, Phys. Rev. Lett. 32 (1974) 882.
[10] A.H. Castro Neto, Phys. Rev. Lett. 86 (2001) 4382.
[11] F.J. Di Salvo, G.W. Hull Jr., L.H. Schwartz, J.M. Voorhoeve, J.V. Waszczak, J. Chem. Phys. 59 (1973) 1922.
[12] A.D. Yoffe, Solid State Ionics 9 (1983) 59.
[13] R.H. Friend, A.D. Yoffe, Adv. Phys. 36 (1987) 1.
[14] L. Fang, Y. Wang, P.Y. Zou, L. Tang, Z. Xu, H. Chen, C. Dong, L. Shan, H.H. Wen, Phys. Rev. B 72 (2005) 014534.
[15] R.M. Fleming, R.V. Coleman, Phys. Rev. Lett. 34 (1975) 1502.
[16] K.E. Wagner, E. Morosan, Y.S. Hor, J. Tao, Y. Zhu, T. Sanders, T.M. McQueen, H.W. Zandbergen, A.J. Williams, D.V. West, R.J. Cava1, Phys. Rev. B 78 (2008) 104520.
[17] X.D. Zhu, Y.P. Sun, X.B. Zhu, X. Luo, B.S. Wang, G. Li, Z.R. Yang, W.H. Song, J.M. Dai, J. Cryst. Growth 311 (2008) 218.
[18] X.D. Zhu, Y.P. Sun, S.B. Zhang, H.C. Lei, L.J. Li, X.B. Zhu, Z.R. Yang, W.H. Song, J.M. Dai, Solid State Commun. 149 (2009) 1296.
[19] M.N. Kunchur, S.J. Poon, Phys. Rev. B 43 (1991) 2916.
[20] J. Bardeen, L.N. Cooper, J.R. Schrieffer, Phys. Rev. 108 (1957) 1175.
[21] N.R. Werthamer, E. Helfand, P.C. Hohenberg, Phys. Rev. 147 (1966) 295.
[22] X.D. Zhu, Y.P. Sun, S.H. Zhang, J.L. Wang, L.J. Zou, L.E. DeLong, X.B. Zhu, X. Luo, B.S. Wang, G. Li, Z.R. Yang, W.H. Song, J. Phys. Condens. Matter 21 (2009) 45701.
[23] W.L. McMillan, Phys. Rev. 167 (1968) 331.